The approximate analytical solution for the top-of-atmosphere spectral reflectance of atmosphere – underlying snow system over Antarctica

A. A. Kokhanovsky

Max Planck Institute for Chemistry, Hahn – Meitner Weg 1, 55128 Mainz, Germany

1. Introduction

The optical signals detected on multiple satellite platforms over snow surfaces are determined by the optical properties of snow surface and atmosphere. The solution of both direct and inverse problems of an atmosphere – underlying snow system requires simple relationships between top-of-atmosphere (TOA) reflectance R and microphysical/optical characteristics of both snow and atmosphere. The task of this paper is to present a simple analytical relationship between the value of R as detected on a satellite with atmosphere/snow properties. Such a relationship can be established using a numerical solution of integro - differential radiative transfer equation (RTE) (Liou, 2022). However, this path is quite complicated and time consuming. The analytical solutions of RTE are needed for the solution of various applied atmospheric and snow optics problems (Cachorro et al., 2022; Mei et al., 2020, 2022; Kokhanovsky, 2021). This is the main driver of this work. To simplify the problem under study we consider the case of Antarctica, where both snow and atmosphere are almost free of pollutants. This work is focused on the simulation of the moderate spectral resolution TOA measurements (1nm or so) and the spectral range 400-1000nm.

In the next section we present the TOA reflectance model. The section 3 is devoted to the application of the model to the measurements performed by the Ocean and Land Colour Instrument (OLCI) on board Sentinel – 3.

Preprints (www.preprints.org) | NOT PEER-REVIEWED | Posted: 15 August 2022 doi:10.20944/preprints202208.0258.v1

2. The top-of-atmosphere reflectance model

2.1.The reflection of light from atmosphere – underlying surface system

The top-of atmosphere spectral reflectance over a Lambertian surface with albedo r_s can be presented in the following way (Liou, 2002; Kokhanovsky et al., 2005a):

$$R = (R_a + \frac{T_a r_s}{1 - r_a r_s})T_g. \quad (1)$$

Here, the values of R_a, r_a, and T_a represent the reflectance, albedo, and total transmittance, respectively, for the artificial atmosphere without gaseous absorbers and black underlying surface, T_g is the gaseous transmittance. The snow is close to the Lambertian surface in the visible. However, there are differences. Therefore, to account for the non-Lambertian effects we substitute the snow albedo in the nominator of Eq. (1) by the snow spectral reflectance R_s. Then it follows (Kokhanovsky et al., 2020):

$$R = (R_a + \gamma T_a R_s)T_g, \quad (2)$$

where $\gamma = (1 - r_a r_s)^{-1}$. It follows from Eq. (2) that $R \to R_s$ at atmospheric optical thickness $\tau \to 0$ outside gaseous absorption bands as it should be. This is because $R_a \to 0, r_a \to 0$ and $T_a \to 1$, $T_g = 1$ in this case by the definition. The errors of Eq. (2) increase with the deviation of the underlying surface from Lambertian one and also with increase of optical thickness τ. Then yet another approach for the account of underlying surface effects on the value of TOA reflectance must be used (see, e.g., Malinka et al., 2016).

However, the focus of this paper is the simulation of satellite optical signals over Antarctica, where τ is small and the error of this approximation is acceptable for the solution of most practical problems related, e.g., to snow remote sensing from space (Kokhanovsky et al., 2019, 2020).

One can see that the desired analytical solution of the problem at hand can be obtained, if analytical equations for all functions in Eq. (2) are used. The analytical solutions for the corresponding functions are considered in the next section.

Preprints (www.preprints.org) | NOT PEER-REVIEWED | Posted: 15 August 2022 doi:10.20944/preprints202208.0258.v1

2.2.The atmospheric path reflectance

The atmospheric path reflectance R_a can be presented in the following way using the Sobolev approximation (Sobolev, 1975; Katsev et al., 2012; Kokhanovsky et al., 2020):

$$R_a = R_{ss} + R_{ms}, \tag{3}$$

where the single scattering contribution can be presented as

$$R_{ss} = M(\tau)p(\theta), \tag{4}$$

$$M(\tau) = \frac{1-\exp(-m\tau)}{4(\mu_0+\mu)}, \tag{5}$$

$$m = \mu_0^{-1} + \mu^{-1}. \tag{6}$$

Here, μ_0 is the cosine of the solar zenith angle (SZA), μ is the cosine of the viewing zenith angle (VZA) , θ is the scattering angle defined as

$$cos\,\theta = -\mu_0\mu + s_0 s\,cos\,\varphi, \tag{7}$$

φ is the relative azimuthal angle (RAA), s_0 is the sine of the SZA, s is the sine of the VZA, τ is the atmospheric optical thickness, $p(\theta)$ is the phase function,

The multiple light scattering contribution R_{ms} can be approximated as (Sobolev, 1975):

$$R_{ms} = 1 + M(\tau)q(\mu_0,\mu) - \frac{N(\tau)}{1+0.75(1-g)\tau}, \tag{8}$$

where

$$N(\tau) = f(\mu_0)f(\mu), \tag{9}$$

$$f(\mu_0) = \frac{1}{2}\left\{1 + \frac{3}{2}\mu_0 + \left(1 - \frac{3}{2}\mu_0\right)\exp\left(-\frac{\tau}{\mu_0}\right)\right\}, \tag{10}$$

$$q(\mu_0,\mu) = 3(1+g)\mu_0\mu - 2(\mu_0+\mu). \tag{11}$$

The value of the average cosine of scattering angle g is determined by the following expression:

$$g = \frac{1}{2}\int_0^\pi p(\theta)\,sin\,\theta\,cos\,\theta\,d\theta. \tag{12}$$

Eq. (8) can be substituted by other approximations or parameterizations (Katkovsky et al., 2018; Mei et al., 2020), if needed.

Preprints (www.preprints.org) | NOT PEER-REVIEWED | Posted: 15 August 2022 doi:10.20944/preprints202208.0258.v1

Eqs. (3), (4), (8) make it possible to calculate the path reflectance analytically for a given phase function $p(\theta)$ and atmospheric optical thickness τ. The approximate account for aerosol absorption effects can be performed multiplying R_{ss} by the single scattering albedo ω_0. It follows from Eq. (8) that $R_{ms} \to 0$ as $\tau \to 0$ as it should be. The accuracy of Sobolev approximation has been studied by many authors including Avaste and Atroshenko (1960), Busbridge and Orchard (1967), and Katsev et al. (2012). It has been found that the error of this approximation is smaller than 10% for most of observation geometries at SZA and VZA smaller than 75 degrees and atmospheric optical thickness smaller than 0.5, which is the case for an atmospheric layer above Antarctica.

The accuracy of the Sobolev approximation presented here increases as $g \to 0$, which is the case for clean atmosphere of Antarctica. Indeed, the atmospheric optical thickness outside gaseous absorption bands can be presented as

$$\tau(\lambda) = \tau_{mol}(\lambda) + \tau_{aer}(\lambda), \tag{13}$$

where λ is the wavelength, τ_{mol} is the molecular optical thickness, τ_{aer} is the aerosol optical thickness (AOT). Let us take the wavelength 400nm. In this case one can assume that $\tau_{mol} = 0.23$ (Tomasi and Petkov, 2015) and $\tau_{aer} = 0.02$ (Six et al., 2005) at Dome C in Antarctica. One can see that atmospheric molecular scatterring and extinction processes are far more important at 400nm as compared to light scattering by atmospheric aerosol.

The atmospheric phase function for a vertically homogeneous nonabsorbing atmospheric layer can be presented as:

$$p(\theta) = \frac{\tau_{mol} p_{mol}(\theta) + \tau_{aer} p_{aer}(\theta)}{\tau_{mol} + \tau_{aer}}, \tag{14}$$

where

$$p_{mol}(\theta) = \frac{3}{4}(1 + cos^2\,\theta) \tag{15}$$

is the molecular scattering phase function and $p_{aer}(\theta)$is the aerosol phase function. It follows from Eqs. (12), (14):

$$g = \frac{\tau_{aer} g_{aer}}{\tau_{mol} + \tau_{aer}}, \tag{16}$$

where g_{aer} is the average cosine of scattering angle for atmospheric aerosol. Taking into account that $g_{aer} \approx 0.7$ at 400nm (Kokhanovsky et al., 2020), we have the following

Preprints (www.preprints.org) | NOT PEER-REVIEWED | Posted: 15 August 2022 doi:10.20944/preprints202208.0258.v1

estimation: $g \approx 0.06$ at Dome C and the proposed approximation for R_{ms} can be used with a high accuracy at 400nm at elevated sites in Antarctica. The value of g somewhat increases at coastal sites being anyway smaller than 0.1-0.2 at 400nm for most of cases. At longer wavelengths, the contribution of multiple scattering decreases and $R_a \to R_{ss}$. Therefore, the errors of the approximation for the value of R_{ms} become irrelevant. This explains the applicability of the Sobolev approximation derived at small values of g for the studied case of Antarctic atmosphere. The approximation can be further improved using the truncation approximation as discussed by Katsev et al. (2012), where also the accuracy of the Sobolev approximation is studied.

We use the following approximation for the spectral aerosol optical thickness (Angström, 1929):

$$\tau_{aer}(\lambda) = \tau_{aer}(\lambda_0)\left(\frac{\lambda}{\lambda_0}\right)^{-\alpha}, \tag{17}$$

where $\lambda_0 = 1\mu m$, and the pair α and $\beta=\tau_{aer}(\lambda_0)$ represent the Angström parameters. The molecular optical thickness is represented as (Iqbal, 1984)

$$\tau_{mol}(\lambda) = \hat{P}\tau_m(\lambda), \tag{18}$$

where $\hat{P} = \frac{P}{P_0}$, P is the site pressure, $P_0 = 1013.25mb$ and $\tau_m(\lambda)$ is approximated by the approximate formular similar to Eq. (17):

$$\tau_{mol}(\lambda) = \tau_m(\lambda_0)\left(\frac{\lambda}{\lambda_0}\right)^{-\upsilon}. \tag{19}$$

One can assume that $\tau_m(\lambda_0) = 0.0084$ and $\upsilon = 4.0932$. Both parameters can vary depending on temperature, humidity and pressure profiles (Hansen and Travis, 1974; Iqbal, 1984; Tomasi et al., 2010; Tomasi and Petkov, 2015). The site pressure at a given altitude *H* can be calculated using the following equation: $P = P_0 \exp\left(-\frac{H}{H_0}\right)$ assuming the scale height H_0 (e.g., *6km).* Alternatively, the value of $\hat{P} = P/P_0$ can be derived from the information on the atmospheric pressure P at a given location (e.g., from the European Centre for Medium-Range Weather Forecasts (ECMWF) re-analysis (https://www.ecmwf.int/en/forecasts/datasets)). We shall assume that the spectral aerosol asymmetry parameter is described by the following formula (Kokhanovsky et al., 2020):

$$g_{aer}(\lambda) = g_0 + g_1 e^{-\frac{\lambda}{\lambda_0}}, \tag{20}$$

Preprints (www.preprints.org) | NOT PEER-REVIEWED | Posted: 15 August 2022 doi:10.20944/preprints202208.0258.v1

where the wavelength λ is in microns and

$$g_0 = 0.5263, g_1 = 0.4627, \lambda_0 = 0.4685\mu m. \quad (21)$$

Taking into account that the spectral TOA reflectance is determined mostly by the underlying snow reflectance for the case of cloudless sky, we can use simplified approximation for the aerosol phase function $p_{aer}(\theta)$ in Eq. (14). This function can be calculated using Mie theory under assumption of aerosol particle size distribution and complex refractive index of aerosol particles or their mixture (van de Hulst, 1981). In this work we assume that the aerosol phase function can be presented in the following analytical form (van de Hulst, 1980):

$$p_{aer}(\theta) = cp_{aer,1}(\theta) + (1-c)p_{aer,2}(\theta), \quad (22)$$

$$p_{aer,1}(\theta) = \frac{1-g_{aer,1}^2}{(1-2g_{aer,1}\cos\theta+g_{aer,1}^2)^{\frac{3}{2}}}, p_{aer,2}(\theta) = \frac{1-g_{aer,2}^2}{(1-2g_{aer,2}\cos\theta+g_{aer,2}^2)^{\frac{3}{2}}}. \quad (23)$$

We shall assume that

$$g_{aer,1} = 0.8, g_{aer,2} = -0.45. \quad (24)$$

It follows for the asymmetry parameter for the case under study:

$$g_{aer} = cg_{aer,1} + (1-c)g_{aer,2} \quad (25)$$

and, therefore,

$$c = \frac{g_{aer}-g_{aer,2}}{g_{aer,1}-g_{aer,2}}, \quad (26)$$

where we assume that g_{aer} is given by Eq. (20). This concludes the description of the approach to derive the atmospheric path reflectance.

2.3 The atmospheric spherical albedo

The atmospheric spherical albedo r_a is found using the approximation for the plane albedo proposed by Sobolev (1975). Namely, he gives the following expression for the atmospheric plane albedo derived using the same technique as used for the determination of the atmospheric path reflectance outlined above:

Preprints (www.preprints.org) | NOT PEER-REVIEWED | Posted: 15 August 2022 doi:10.20944/preprints202208.0258.v1

$$r_p(\mu_0) = 1 - \frac{f(\mu_0)}{1 + 0.75(1-g)\tau}, \tag{27}$$

where $f(\mu_0)$ is given by Eq. (10) and light absorption processes are neglected. It follows from Eq. (27) as $\tau \to 0$:

$$r_p(\mu_0) = w\tau, \tag{28}$$

where $w=(2\mu_0)^{-1}$- $0.75g$, which is a valid approximation at small values of g. In particular, Eq. (28) coincides with a similar formula given by Coakley and Chylek (1975) and Wiscombe and Grams (1976) for the case of g=0.

The spherical albedo is defined as

$$r_a = 2\int_0^1 r_p(\mu_0)\,\mu_0 d\mu_0 . \tag{29}$$

The substitution of Eq. (27) to Eq. (29) gives after integration:

$$r_a = 1 - \frac{1 + \psi(\tau)}{1 + 0.75(1-g)\tau}, \tag{30}$$

where

$$\psi(\tau) = \left[1 + \frac{\tau}{2}\right]\frac{\tau^2}{2}E_1(\tau) - \left[1+\tau\right]\frac{\tau}{4}\exp(-\tau) \tag{31}$$

and

$$E_1(\tau) = \int_1^\infty \frac{\exp(-x\tau)}{x}\,dx \tag{32}$$

is the exponential integral (Abramowitz and Stegun, 1964). The exponential integral has the following properties (Abramowitz and Stegun, 1964; van de Hulst, 1980) :

$$E_1(\tau \to \infty) = \exp(-\tau)/\tau \to 0, \tag{33}$$

$$\tau E_1(\tau \to 0) = \tau^2 - \frac{\tau^3}{4} + \frac{\tau^4}{18} - \frac{\tau^5}{96} - \tau\ln\tau - \gamma\tau, \tag{34}$$

Preprints (www.preprints.org) | NOT PEER-REVIEWED | Posted: 15 August 2022 doi:10.20944/preprints202208.0258.v1

where $\gamma = 0.5772157$ is the Euler's constant. Therefore, one can see that $r_a \to 1$ as $\tau \to \infty$ as it should be for nonabsorbing case considered here.

The atmospheric optical thickness is usually smaller than 0.5 for polar atmospheres and one can use the approximation given by Eq. (34) for the product $\tau E_1(\tau)$ in Eq. (31). Then it follows:

$$\psi(\tau) = \frac{1}{2}\left(\tau + \frac{\tau^2}{2}\right)\left(\tau^2 - \frac{\tau^3}{4} + \frac{\tau^4}{18} - \frac{\tau^5}{96} - \tau\ln\tau - \gamma\tau\right) - \frac{1}{4}(1+\tau)\tau\exp(-\tau). \quad (35)$$

Therefore, one derives:

$$r_a = 1 - \left[\frac{1 - \frac{\tau}{4}(1+\tau)\exp(-\tau) + \frac{\tau^2}{2}\left(1+\frac{\tau}{2}\right)\left(\tau - \frac{\tau^2}{4} + \frac{\tau^3}{18} - \frac{\tau^4}{96} - \ln\tau - \gamma\right)}{1 + 0.75(1-g)\tau}\right]. \quad (36)$$

It follows from Eq. (36) as $\tau \to 0: r_a \to b\tau$, where $b = 1 - 3g/4$. One can see that $r_a \approx \tau$ at small values of atmospheric optical thickness and g=0. The value of $r_a < \tau$ at g> 0.

The intercomparison of the dependence of spherical albedo on the value of atmospheric optical thickness derived using Eq. (36) and exact radiative transfer calculations is shown in Fig.1, where we also present the results derived using the following simple formula (approximation – 2) valid for the case of pure molecular scattering (Kokhanovsky et al., 2005a):

$$r_a = \tau(a\exp(-\tau/\alpha) + b\exp(-\tau/\beta) + c), \quad (37)$$

where *a=0.180, b=0.583, c=0.215,* α *=0.168,* β *=1.092*. The maximal error of Eq. (37) is smaller than 1%. It is based on the parameterization of exact radiative transfer (RT) calculations for the case of molecular scattering (Kokhanovsky et al., 2005). The error of approximation (36) is smaller than 2% at $\tau \le 1$ for the molecular scattering case. We also show the calculations for the case of aerosol and molecular scattering mixture. It is assumed that aerosol optical thickness is 0.05 and molecular optical thickness changes from 0.01 till 1.0. The aerosol parameters were taken the same as in the paper of Kokhanovsky et al. (2010). One can see that the errors of the approximation do not increase substantially in the presence of a thin aerosol layer. It should be pointed out that one is interested not in the value of r_a but rather in the

Preprints (www.preprints.org) | NOT PEER-REVIEWED | Posted: 15 August 2022 doi:10.20944/preprints202208.0258.v1

quantity $\gamma = (1 - r_a r_s)^{-1}$ in the problem under study (see Eq. (2)). The error of an approximation for the value of γ is even lower.

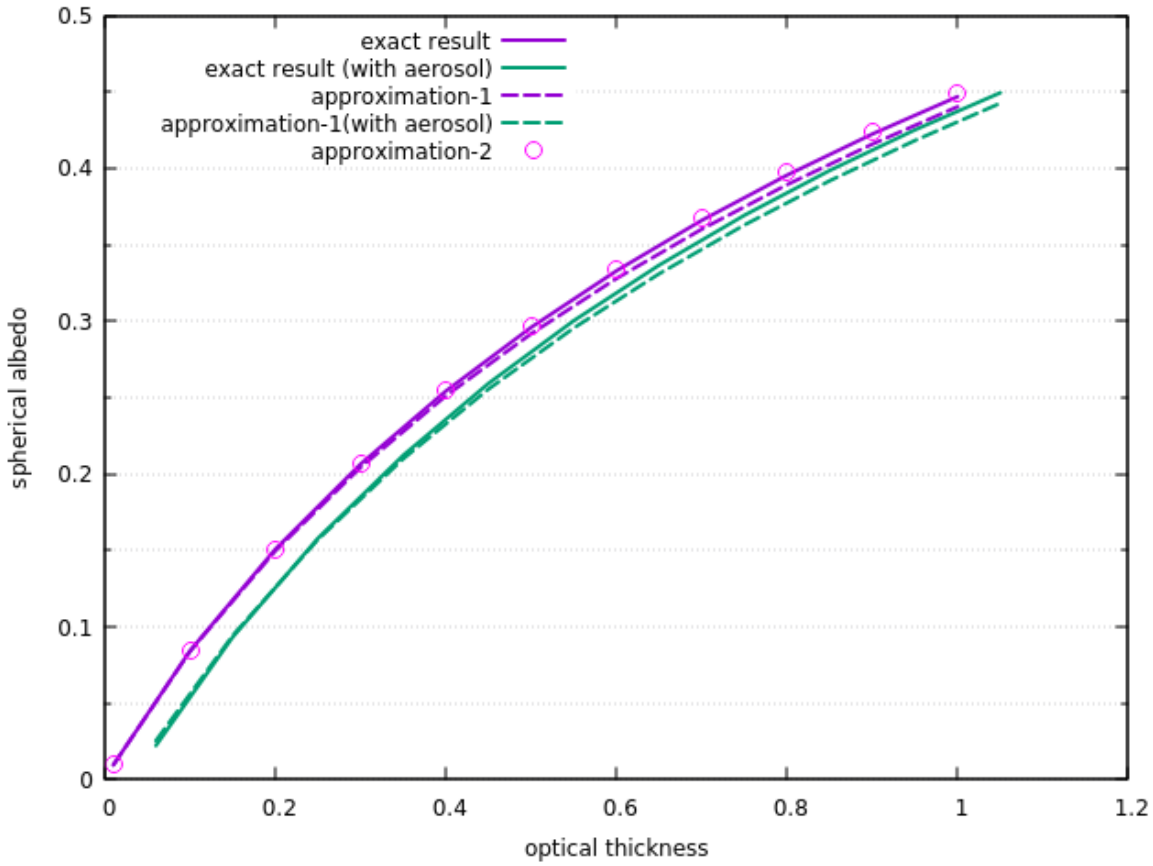

Fig.1. The intercomparison of different approximations for the calculation of the spherical albedo of atmosphere with molecular scattering with different values of atmospheric optical thickness. The exact RT calculations have been performed using the SORD code (Korkin et al., 2018).

2.4 The atmospheric transmittance outside gaseous absorption bands

The transmission function T_a is approximated as follows (Katsev et a l., 2012):

$$T_a = t_a^m, \tag{38}$$

Preprints (www.preprints.org) | NOT PEER-REVIEWED | Posted: 15 August 2022 doi:10.20944/preprints202208.0258.v1

where *m* is given by Eq. (6). The value of t is calculated using the following approximation (Katsev et al., 2012):

$$t_a = e^{-B\tau}. \tag{39}$$

Here,

$$B = \frac{1}{2}\int_{\frac{\pi}{2}}^{\pi} p(\theta)\, sin\,\theta\, d\theta \tag{40}$$

is the so – called backscattering fraction. The substitution of Eq. (14) to Eq. (40) gives:

$$B = \frac{\tau_{mol}B_{mol}+\tau_{aer}B_{aer}}{\tau_{mol}+\tau_{aer}}, \tag{41}$$

where $B_{mol} = 0.5$,

$$B_{aer} = cB(g_{aer,1}) + (1-c)B(g_{aer,2}) \tag{42}$$

and

$$B(G) = \frac{1-G}{2G}\left[\frac{1+G}{\sqrt{1+G^2}} - 1\right]. \tag{43}$$

It follows at small values of G:

$$B(G) \approx \frac{1}{2} + \frac{G(G^2-3)}{2(1+G^2+(1-G^2)\sqrt{1+G^2})}. \tag{44}$$

The accuracy of Eqs. (38) – (40) has been studied by Katsev et al. (2012), where it has been found this approximation can be used with the accuracy better than 5% at solar zenith angles smaller than 70 degrees for the continental and water soluble aerosol layers with aerosol optical thickness smaller than 0.5, which is the case for polar atmospheres.

2.5 The atmospheric gaseous transmittance

Atmospheric gaseous transmittance in Eq. (2) can be presented as a product of transmittances due to various gaseous components of the atmosphere. In this work we are interested primarily in the calculation of radiative characteristics in the range 400-1000nm, where main atmospheric gases, which contribute significantly to the atmospheric absorption processes are molecular oxygen, ozone, and water vapour. Therefore, to simplify the calculations, the contribution of

Preprints (www.preprints.org) | NOT PEER-REVIEWED | Posted: 15 August 2022 doi:10.20944/preprints202208.0258.v1

other gases is ignored. Such an approach has been also used in several previous papers on the subject (Katkovsky et al., 2018; Cachorro et al., 2022). In particular, we shall assume that the gaseous transmittance is given by the following product:

$$T_g = T_{O_2} T_{O_3} T_{H_2O}, \tag{45}$$

where T_{O_2}, T_{O_3}, and T_{H_2O} are the gaseous transmittances due to molecular oxygen, ozone and water vapour.

2.5.1 Ozone

We shall assume that the ozone transmittance T_{O_3} can be derived using the following expression (Iqbal, 1984; Kokhanovsky et al., 2021a):

$$T_{O_3} = \exp(-m_{O_3} \tau_{O_3}(\lambda)), \tag{46}$$

where m_{O_3} is the ozone airmass factor (AMF) and $\tau_{O_3}(\lambda)$ is the vertical optical density (VOD) of ozone:

$$\tau_{O_3}(\lambda) = \int_0^{z_{top}} C_{abs,O_3}(\lambda, z) n_{O_3}(z) dz, \tag{47}$$

where $C_{abs,O_3}(\lambda, z)$ is the ozone absorption cross section, z is the altitude, z_{top} is the top of atmosphere altitude, $n_{O_3}(z)$ is the number concentration of ozone molecules at the altitude z.

We use the geometrical approximation for the AMF (see Eq. (6)). In the spectral region of interest the dependence of the ozone absorption cross section on both temperature and pressure (and, therefore, the altitude) can be ignored. Then one derives from Eq. (47):

$$\tau_{O_3}(\lambda) = N C_{abs,O_3}(\lambda), \tag{48}$$

where

$$N_{O_3} = \int_0^{z_{top}} n_j(z) dz \tag{49}$$

Preprints (www.preprints.org) | NOT PEER-REVIEWED | Posted: 15 August 2022 doi:10.20944/preprints202208.0258.v1

is the total ozone column (TOC) measured in molecules per cm^2. The value of C_{abs,O_3} is measured in cm^2 (per molecule) and can be parameterized as follows in the spectral range under study (Green et al., 1988):

$$C_{abs,O3}(\lambda) = AF(\lambda), \tag{50}$$

where $A = 18.48 \times 10^{-21} cm^2$ /molecule

$$F(\lambda) = \frac{\zeta(\lambda)}{(1+\zeta(\lambda))^2}, \tag{51}$$

$$\zeta = \exp(\frac{w(\lambda) - w_p}{\Delta}), \tag{52}$$

$w = 10^7 / \lambda$, where λ is given in nm and w is the wavenumber with the dimension cm^{-1}. The authors suggest (after correction of a misprint) the following values for the parameters in Eq. (52): $w_p = 16811 cm^{-1}$, $\Delta = 877 cm^{-1}$ (at wavenumbers $w < w_p$) and $\Delta = 1210 cm^{-1}$ at $w \geq w_p$. We show the results of calculations of $C_{abs,O3}(\lambda)$ according to this equation and also measurements of $C_{abs,O3}$ (Gorshelev et al., 2012) in Fig.2a as the function of the wavelength $\lambda = 10^7 / w$, where w is given in 1/cm and the dimension of the wavelength is nm. One can see that theoretical and experimental results differ in the regions, where the spectral curve $C_{abs,O3}(\lambda)$ has oscillations. The relative accuracy is better than 25% in the spectral range 500-700nm (see Fig.2b), which suits our purposes (especially because we are interested in the value of exp(- $m\tau_{O_3}$), which is derived with much better accuracy as compared to the ozone VOD). Summing up, we assume that the value of T_{O_3} can be approximated as follows:

$$T_{O_3} = \exp(-\varsigma F(\lambda)), \tag{53}$$

where $\varsigma = A m_{O_3} N_{O_3}$. The error of the ozone transmittance calculation using simple Eq. (53) as compared to the case, where experimental values of $C_{abs,O3}$ are used is shown in Fig.3 at N_{O3} =300DU (1DU=2.69× 10^{16} ozone molecules/ cm^2) and the ozone airmass factor m_{O_3} =1. One can see that the respective error is below 1% for the case studied, which is smaller than the error of the respective spectral reflectance measurements.

Preprints (www.preprints.org) | NOT PEER-REVIEWED | Posted: 15 August 2022 doi:10.20944/preprints202208.0258.v1

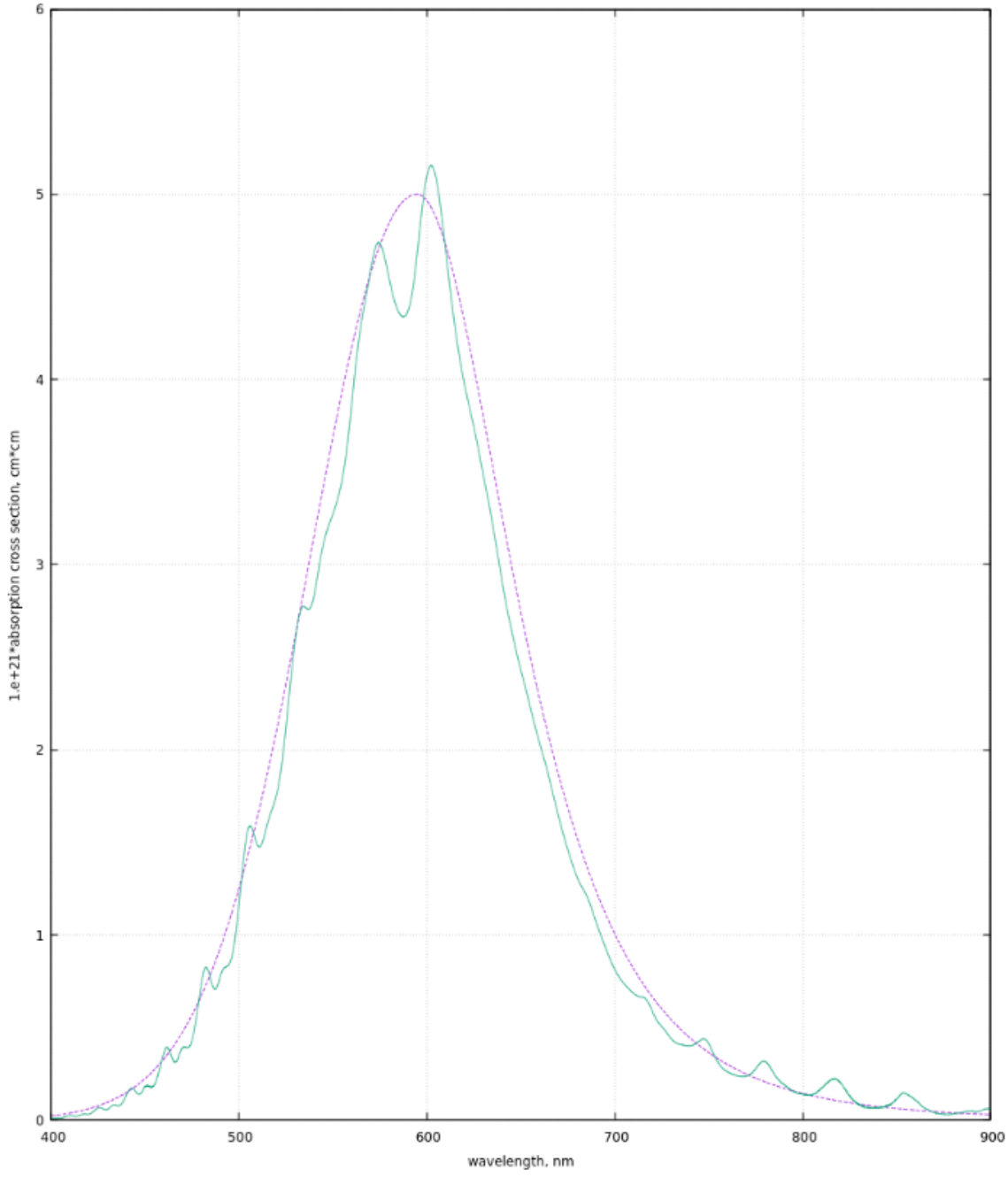

Fig.2a. The intercomparison of modelled (dashed) and experimentally measured (solid line) ozone absorption cross section (at temperature t=233K).

Preprints (www.preprints.org) | NOT PEER-REVIEWED | Posted: 15 August 2022 doi:10.20944/preprints202208.0258.v1

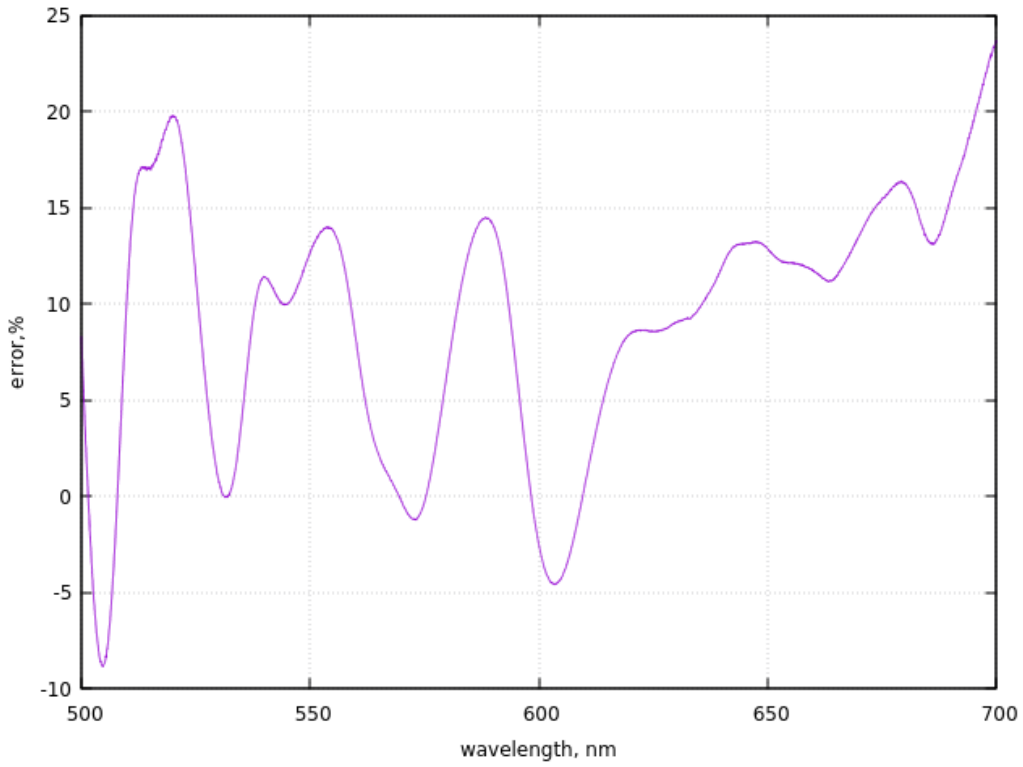

Fig.2b. The error of the approximation for the ozone VOD.

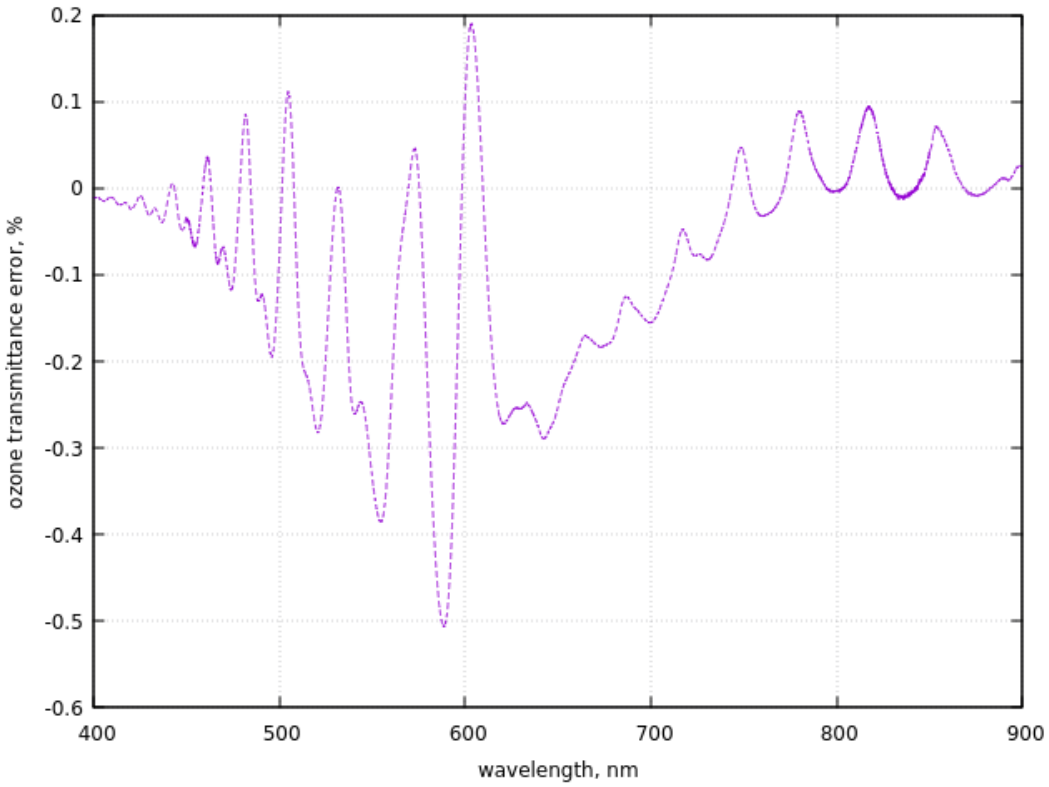

Fig.3. The ozone transmittance error.

Preprints (www.preprints.org) | NOT PEER-REVIEWED | Posted: 15 August 2022 doi:10.20944/preprints202208.0258.v1

2.5.2 Water vapor

The transmittance of water vapour in the spectral range 900-1000nm can be calculated using the following simple equation (Green et al., 1988):

$$T_{H_2O} = \exp\left\{-s^{x_1}\right\}, \tag{54}$$

where

$$s = N_{H_2O}^{ef} c_{H_2O}(\lambda), \tag{55}$$

$$N_{H_2O}^{ef} = Q_{H_2O} m_{H_2O} N_{H_2O} \ , \tag{56}$$

$$Q_{H_2O} = (\bar{P} / P_0)^n (t_0 / \bar{t})^k \ , \tag{57}$$

$$c_{H_2O}(\lambda) = \sum_{j=1}^{2} B_j F_j(\lambda), \tag{58}$$

$$F_j(\lambda) = \frac{\zeta_j(\lambda)}{(1+\zeta_j(\lambda))^2}, \qquad \zeta_j(\lambda) = \exp(\frac{w(\lambda) - w_j}{\Delta_j}), \tag{59}$$

$w = 10^7 / \lambda$, where λ is given in nm and w is the wavenumber with the dimension cm^{-1}, n=0.775, k=0.721, t_0 =273.16K, P_0 =1013.25hPa, $(\bar{P}, \bar{t})$ are average values of pressure and temperature for a given location calculated using respective vertical profiles, $x_1 = 0.649$, m_{H_2O} is the water vapour airmass factor, which can be found using geometrical approximation (see Eq. (6)). The constants B_j, w_j and Δ_j are given in Table 1 below. The value of the Precipitable Water Vapour (PWV) content N_{H_2O}, which is input parameter for the model, is given in cm. When measured in linear units (cm, mm), water vapour column is represented by the height (or depth) N_{H_2O} of the water column would occupy if the vapor were condensed into liquid and spread evenly across the column. Using the density of water, we can also report water vapor in gcm^{-2} = 1 cm or kgm^{-2} =1mm. The example of water vapour gaseous transmittance calculated in the framework of this model is presented in Fig.4.

Eq. (54) is similar to Eq. (53) except x_1 and Q ***differ from unity*** as assumed in Eq. (54). This difference is due to the fact that most of ozone is located in a single layer positioned in stratosphere, which is not the case for water vapor with largest concentrations closer to the

Preprints (www.preprints.org) | NOT PEER-REVIEWED | Posted: 15 August 2022 doi:10.20944/preprints202208.0258.v1

surface. The value of the effective PWV content $N_{H_2O}^{ef}$ can be estimated from Eqs. (56), (57) under assumption that the value of Q_{H_2O} is known. The determination of N_{H_2O} requires information on water vapour airmass factor and also temperature and pressure profiles for a given location.

Table 1. The parameters of water vapour absorption model (Green et al., 1988)

λ, nm	B_j, cm^{-1}	w_j, cm^{-1}	Δ_j, cm^{-1}	Comment
910 (j=1)	0.744	11099	23.4 $(w < w_j)$ 73.8 $(w \geq w_j)$	Weak absorption band
940 (j=2)	7.560	10697	23.1 $(w < w_j)$ 110.2 $(w \geq w_j)$	Strong absorption band

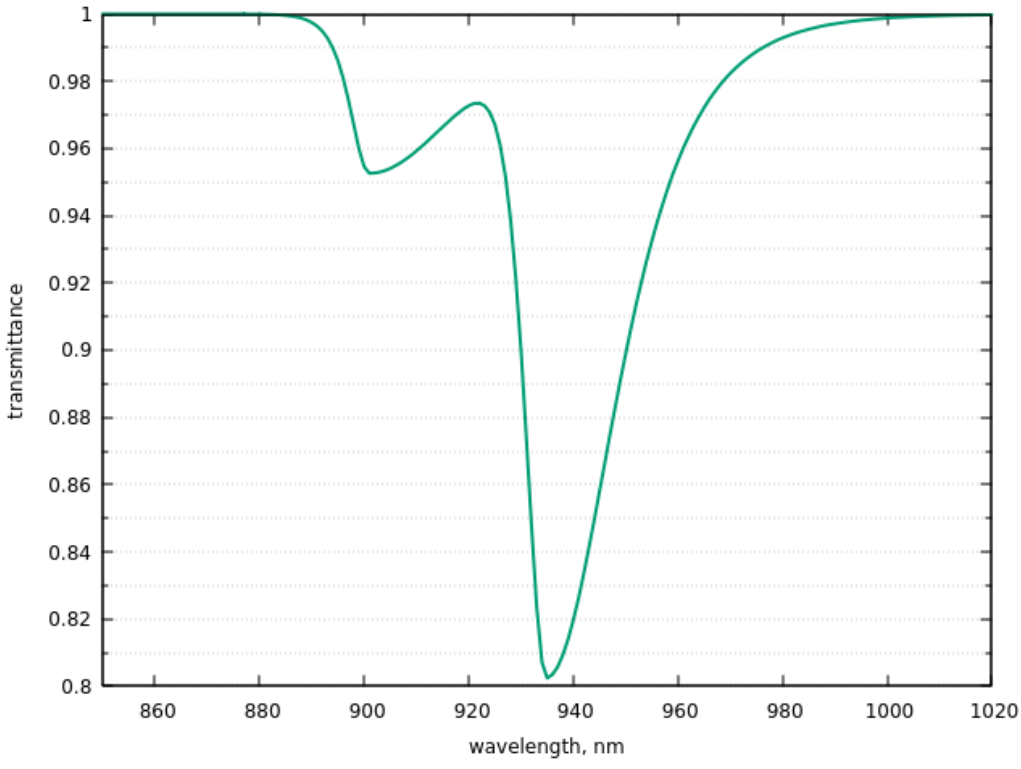

Fig.4. Water vapor transmittance at N_{H_2O} =0.33mm, $\bar{t} = 233K$, $\bar{P} = 325hPa$, $m_{H_2O} = 3.32$.

Preprints (www.preprints.org) | NOT PEER-REVIEWED | Posted: 15 August 2022 doi:10.20944/preprints202208.0258.v1

2.5.3 Oxygen

The oxygen transmittance is found using the approximation similar to Eq. (54) (Pierluissi and Tsai, 1986):

$$T_{O_2} = \exp(-s^{x_2}), \tag{60}$$

where

$$s = N_{O_2}^{ef} c_{O_2}(\lambda), \tag{61}$$

$$N_{H_2O_2}^{ef} = Q_{O_2} m_{O_2} N_{O_2} \tag{62}$$

The parameter Q_{O_2} is given by formula similar to Eq. (57) except *n=0.9353, k=0.1936,* m_{O_2} is the oxygen AMF, which can be estimated using geometrical approximation (see Eq.(6)), N_{O_2} is the oxygen amount in atm-cm, x_2*=0.5641*.

The spectral function $c_{O_2}(\lambda)$ has been tabulated by Pierluissi and Tsai (1986). We have parameterized this function using the double Gauss approximation (at the wavelengths smaller or equal 764nm):

$$, c_{O_2}(\lambda) = \Lambda \exp(-1.7(\lambda - \lambda_1)^2) + 0.32\Lambda \exp(-0.7(\lambda - \lambda_2)^2), \tag{63}$$

where λ_1=760.75nm, $\lambda_2 = 763.36nm$, $\Lambda = 1.8 \times 10^{-5}$ (cm-atm)$^{-1}$ and λ is expressed in nm. At the wavelengths λ larger than 764nm, the following parameterization has been used:

$$c_{O_2}(\lambda) = \frac{\Upsilon}{1 + \exp\left[(\lambda - \lambda_s)/\Delta_s\right]}, \tag{64}$$

where $\Upsilon = 8.419 \times 10^{-6}$ (cm-atm)$^{-1}$, λ_s=764.11nm, Δ_s=0.85036nm. The intercomparison of $c_{O_2}(\lambda)$ derived using Eqs. (63), (64) and data presented by Pierluissi and Tsai (1986) is shown in Fig.5. It follows that the proposed parameterizations can indeed be used to model gaseous transmittance in the molecular oxygen A-band. The transmittance $T_{O_2}(\lambda)$ at N_{O_2} =8.706853× 10^5 cm-atm and $m_{O_2} = 1$ is given in Fig.6 both using Eqs. (63), (64) and tabular data for the spectral function given by Pierluissi and Tsai (1986). Good correspondence between two approaches for the calculation of $T_{O_2}(\lambda)$ is found.

Preprints (www.preprints.org) | NOT PEER-REVIEWED | Posted: 15 August 2022 doi:10.20944/preprints202208.0258.v1

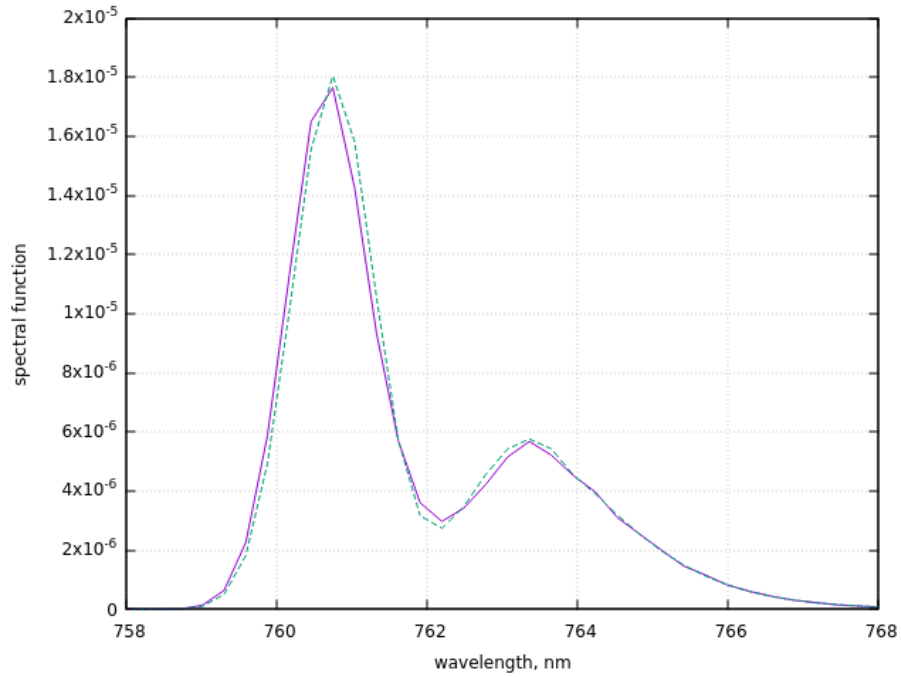

Fig.5. The spectral function tabulated by Pierluissi and Tsai (1986) (solid line) and derived using Eq. (63), (64) (dashed line).

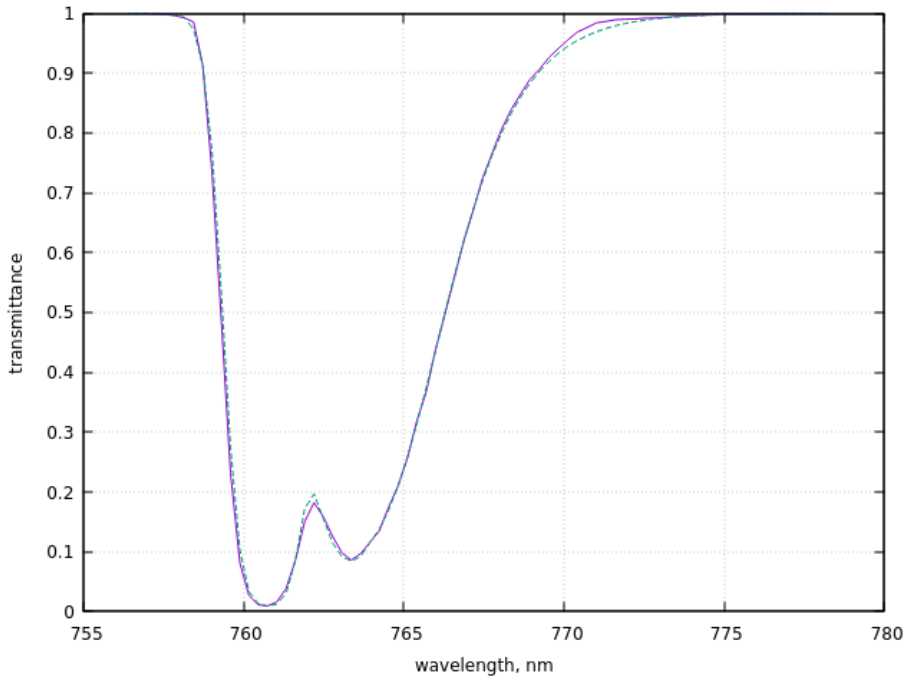

Fig.6. The oxygen transmittance (solid line – the tabular data of Pierluissi and Tsai (1986) are used, dashed line - Eqs. (63), (64) for the spectral function are used).

Preprints (www.preprints.org) | NOT PEER-REVIEWED | Posted: 15 August 2022 doi:10.20944/preprints202208.0258.v1

2.6 Reflectance of solar light from a snow surface

The only function in Eq. (2), which we did not study so far is the spectral snow reflectance $R_s(\lambda)$. It is modelled using the approximation proposed by Zege et al. (1991), Kokhanovsky and Zege (2004) and Kokhanovsky et al. (2018, 2019, 2021b) for the case of clean vertically and horizontally homogeneous plane – parallel layers of turbid media:

$$R_s(\mu,\mu_0,\varphi) = R_0(\mu,\mu_0,\varphi) r_s^{\xi}\,, \tag{65}$$

where

$$\xi = u(\mu_0)u(\mu)/R_0(\mu,\mu_0,\varphi), \tag{66}$$

$$u(\mu_0) = \frac{3}{5}\mu_0 + \frac{1+\sqrt{\mu_0}}{3}\,, \tag{67}$$

$$r_s = exp\{-\sqrt{y}\ \}, \tag{68}$$

$$y = L\alpha_i, \tag{69}$$

$$R_0 = \frac{a + b(\mu_0+\mu_0) + c\mu_0\mu + p_s(\theta)}{4(\mu_0+\mu)} \tag{70}$$

where a = 1.247, b = 1.186, c = 5.157, $\alpha_i = \frac{4\pi\chi}{\lambda}$ is the bulk ice absorption coefficient, χ is the imaginary part of complex ice refractive index (Kokhanovsky, 2021), L is the effective absorption length (proportional to the average ice grain size). The phase function of a snow layer $p_s(\theta)$ is approximated as (Kokhanovsky, 2005b, 2021):

$$p_s(\theta) = 11.1\exp(-0.087\theta) + 1.1\exp(-0.014\theta), \tag{71}$$

where θ is the scattering angle in degrees.

In the case of polluted snow the equations given below remain valid except the parameter y is changed to the following expression (Kokhanovsky et al., 2018, 2021b):

$$y = L\left[\alpha_i + f(\lambda/\lambda_0)^{-\upsilon}\right], \tag{72}$$

where υ is the absorption Angström parameter of impurities in snow, λ_0 =1μm and f is the parameter, which is the proportional to the relative impurity concentration $C = C_{imp}/C_{ice}$,

Preprints (www.preprints.org) | NOT PEER-REVIEWED | Posted: 15 August 2022 doi:10.20944/preprints202208.0258.v1

where C_{imp} is the volumetric concentration of impurities, C_{ice} is the volumetric concentration of ice grains. Namely, it follows (Kokhanovsky et al., 2021b):

$$f = \frac{C}{K}\kappa_0, \tag{73}$$

where K is the absorption enhancement parameter (≈ 1.8) and κ_0 is the volumetric absorption coefficient of impurities at the wavelength 1μm. The value of κ_0 is equal to the ratio of average absorption cross section of impurities (say, dust particles) to their average volume (Kokhanovsky et al., 2021b). One can see that the description of optical characteristics of polluted snow requires two additional parameters (f, υ).

3. The intercomparison of derived parameterization with spaceborne measurements of spectral top-of-atmosphere reflectance

The TOA spectral reflectance function calculated using Eq. (2) is given in Fig. 7. We also show the simulation and measurement results for the top-of-atmosphere OLCI (https://sentinels.copernicus.eu/web/sentinel/technical-guides/sentinel-3-olci) reflectance at Dome C in Antarctica. The specification of both OLCI channels and their widths is used in the averaging procedure (assuming box function). The derived bottom of atmosphere (BOA) snow reflectance is also shown for the comparison. The TOA reflectance measured by OLCI is given by crosses on Fig.7. The assumed parameters of atmosphere – underlying snow system are given in Table 2. The molecular optical thickness has been modelled using the following equation:

$$\tau_{mol} = 0.015 + 20.64\exp(-\lambda/86.16), \tag{74}$$

where λ is the wavelength in nm. Eq. (74) has been derived using fitting the spectral molecular optical thickness tabular data provided by Tomasi and Petkov (2015) for the case of Dome C conditions.

The spectral imaginary part of ice refractive index has been found as proposed by Kokhanovsky (2021) using the dataset of Picard et al. (2016) at the wavelengths below 600nm and that given by Warren and Brand (2008) at larger wavelengths. The linear interpolation has been applied to derive the values between the spectral grid points presented in respective tables.

Preprints (www.preprints.org) | NOT PEER-REVIEWED | Posted: 15 August 2022 doi:10.20944/preprints202208.0258.v1

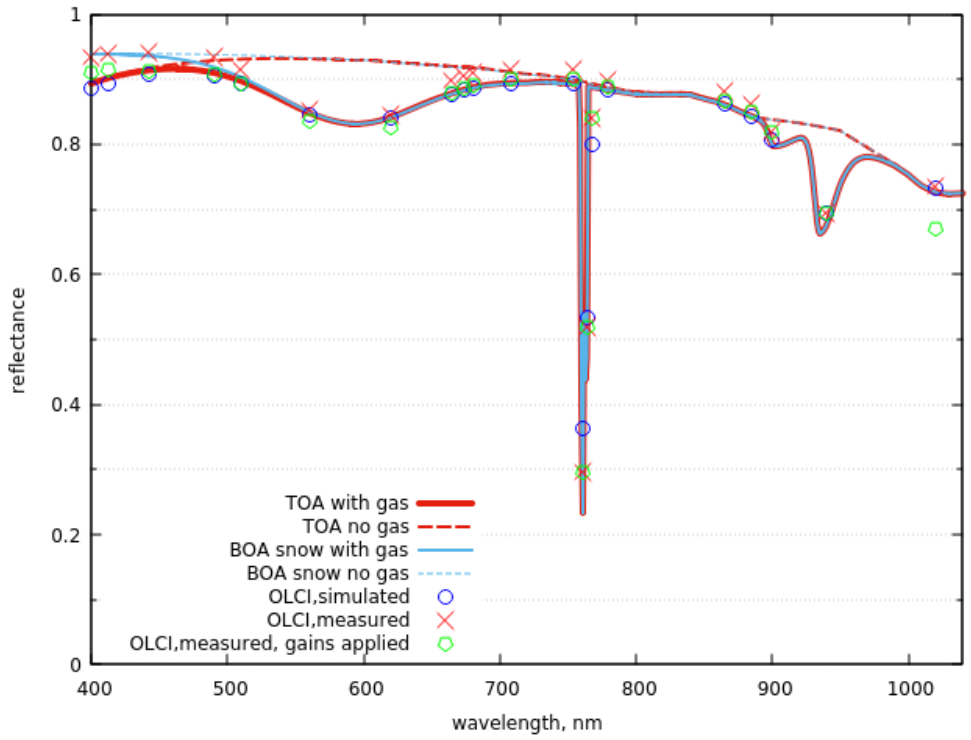

Fig.7. The spectral TOA reflectance measured by OLCI (symbols) and also modelled using Eq. (2) (solid red line). Dashed red line corresponds to the artificial atmosphere without gas. Blue dashed line corresponds to the case, when atmospheric contribution is neglected. Solid blue line corresponds to the case, when absorption by atmospheric gases (but not light scattering in atmosphere) is fully accounted for. The solar zenith angle is equal to 63.61 degrees, the VZA is 20.63 degrees and the relative azimuthal angle is 118.39 degrees. The satellite measurements have been performed on November 10, 2017 at Dome C (Antarctica) under geometry specified above.

Fig.7 shows that OLCI spectra are significantly influenced by the gaseous absorption. The decrease of OLCI spectra towards 400nm is due to atmospheric light scattering. This decrease can be used to estimate the atmospheric aerosol load over snow for elevated atmospheric aerosol load conditions. As a matter of fact, the aerosol load in Antarctica is in general too low (Six et al., 2005) to be measured from a satellite taking into account instrument calibration errors and inaccuracy of bottom-of-atmosphere albedo estimations. The influence of atmospheric scattering can be neglected at the wavelengths above 500nm for the case studied. Measurements at 1020nm are affected by the light absorption effects in snow cover with larger values of reflectance for smaller and less absorbing ice grains. Measurements in the vicinity of ozone (600nm) and water vapour (940nm) absorption bands can be used to estimate the total ozone

Preprints (www.preprints.org) | NOT PEER-REVIEWED | Posted: 15 August 2022 doi:10.20944/preprints202208.0258.v1

Table 2. The parameters of the model used in Fig.7 for the case of clean snow underlying surface.

N	parameter	value	comment
1	α	0.008	atmospheric aerosol
2	β	1.3	atmospheric aerosol
3	N_{O_2}, cm-atm	8.706853×10^4	oxygen
4	N_{O_3}, DU	250	ozone
5	N_{HO_2}, mm	0.33	water vapour
6	P, hPa	650	surface pressure
7	$\bar{P}$, hPa	325	average pressure
8	$\bar{t}$, K	233	average temperature
9	L, *mm*	2.24	snow effective absorption length

Preprints (www.preprints.org) | NOT PEER-REVIEWED | Posted: 15 August 2022 doi:10.20944/preprints202208.0258.v1

and the atmospheric precipitable water vapour content. They can be derived from the depth of corresponding absorption bands as seen in the reflected light (Kokhanovsky et al., 2021; Preusker et al., 2021). The atmospheric oxygen column is known in advance for any height of underlying surface. Therefore, the measurements of reflectance in the oxygen A-band can be used to estimate the height of underlying surface, ground atmospheric pressure and develop various cloud screening procedures.

We have found that the difference of theoretical results derived using Eq. (2) and observations for all channels is smaller than 5% except for the channel corresponding to the maximal absorption by oxygen in the OLCI spectrum, where one needs to use the instrument spectral response function (instead of box function) in the averaging procedure. It should be pointed out that some differences seen in Fig.7 are due to errors of OLCI measurements. In particular, theoretical results suggest that the spectral reflectance must decrease in the range 400-450nm (towards shorter wavelength). This is mostly due to molecular light scattering effects for the case studied. Such a decrease is not seen in the OLCI spectrum given in Fig.7 by red crosses, which makes it possible to suspect the problem with OLCI measurements in this spectral range. As a matter of fact, such anomaly in OLCI spectra has already been detected. In particular, Marezan and Rueskas (2020) have proposed to use OLCI calibration coefficients (gains), which leads to the decrease of OLCI reflectance in the range 400-450nm and change of OLCI spectral reflectance at some other channels. As it follows from Fig.7, the difference between modelled and measured spectra decreases after application of gains (except for the last channel). The difference at the last OLCI channel is due to the fact that the value of L in Table 2 has been derived from OLCI measurements without application of gains. This difference is reduced in case the value of L is retrieved from the measurements at the last OLCI channel after application of the gains.

The total ozone column and precipitable water vapour content are also important atmospheric parameters, which can be found. It follows that the value of TOC=250DU for the case shown in Fig.7. ECMWF data for DOME C provided in OLCI files at this date and time give: TOC=291DU. Therefore, the difference is around 14% for the TOC for the case studied. The study of errors related to the determination of TOC from OLCI measurements has been performed by Kokhanovsky et al. (2021a). The derived value of PWV for the case shown in Fig. 7 is 0.33mm. This value is close to the average value of PWV at the site for autumn (PWV=0.4mm), where averaging has been performed for 4 years (2010-2014, see Table 4 presented by Ricaud et al. (2010)). Further discussion of the PWV content as retrieved using

Preprints (www.preprints.org) | NOT PEER-REVIEWED | Posted: 15 August 2022 doi:10.20944/preprints202208.0258.v1

OLCI over land surfaces and related errors including the influence of instrumental effects on the retrieval is given by Preusker et al. (2021).

As a matter of fact, the theory presented above makes it possible to estimate the product X=*mQN* accurately. The correct value of *N* can be derived from X: *N*=X/*Qm* using improved estimation of the AMF *m* and also the parameter *Q*. The further discussion of this topic is out of scope of this paper.

The effective grain size can be derived from the value of the effective absorption length using the following approximate equation (Kokhanovsky et al., 2022): *d=L/16*. Therefore, the effective grain diameter *d*=0.14mm for the case shown in Table 2, which is consistent with grain size measurements in Antarctica as reported by Gray et al. (2022).

We also applied the theory described above to a large OLCI dataset in the Eastern Antarctica. Fig.8 shows the distribution of the coefficient of variance (normalized root-mean-square difference between model and spaceborne measurements of TOA reflectance outside oxygen absorption band):

$$CV = \frac{RMSD}{\bar{R}}, \tag{75}$$

where

$$RMSD = \sqrt{\frac{\sum_{j=1}^{J}(R_{appr}(\lambda_j) - R_{meas}(\lambda_j))^2}{J}}, \tag{76}$$

$$\bar{R} = \frac{\sum_{j=1}^{J} R_{meas}(\lambda_j)}{J}, \tag{77}$$

and *J=18* (oxygen absorption A- band measurements are excluded). As it follows from the comparison of Figs. 8, 9, the largest values of CVs are correlated with the largest values of OLCI reflectance in oxygen A-band signifying the presence of clouds (Kokhanovsky, 2006). The parameters L, N_{O_3}, $N_{H_2O}^{ef}$ for the OLCI scene studied have been estimated using the following equations, which follow from Eqs. (2), (46), (54), (65) under assumption that atmospheric scattering contribution is neglected (Kokhanovsky et al., 2019, 2021a):

Preprints (www.preprints.org) | NOT PEER-REVIEWED | Posted: 15 August 2022 doi:10.20944/preprints202208.0258.v1

$$L = \frac{\ln^2(R_0 / R_{21})}{\alpha_{21}\xi^2}, \tag{78}$$

$$N_{O_3} = \mathrm{K}\frac{\ln(R_{s,7} / R_7)}{m_{O_3}}, \tag{79}$$

$$N_{H_2O}^{ef} = \ln^{\varepsilon}(R_{s,20} / R_{20}), \tag{80}$$

where K =9349.3DU, $\varepsilon = 1/x_1$, $\alpha_{21} = \frac{4\pi\chi_{21}}{\lambda_{21}}$ is the bulk ice absorption coefficient at 1020nm, χ_{21} is the imaginary part of the ice refractive index at the OLCI channel $\lambda_{21} = 1020nm$, ξ is given by Eq. (66), R_7, R_{20}, R_{21} are the OLCI TOA measurements at the wavelengths 620, 940 and 1020nm, respectively, $R_{s,7}$ $R_{s,20}$ $R_{s,21}$ are the estimated OLCI TOA reflectances at the OLCI channels 7 (620nm), 20 (940nm) and 21 (1020nm). Air mass factors in Eqs. (79), (80) are estimated using the geometrical approximation. The value of molecular optical thickness has been modelled using Eq. (74). The imaginary part of ice refractive index has been found as specified above. The parameter $N_{O_2}^{ef}$ has been estimated using the formula similar to Eq. (80) except OLCI measurements and snow reflectance at the channel 764.38nm have been used. Other parameters have been selected as specified in Table 2.

To increase the accuracy of the derived spectral reflectance one can substitute the approximate value of R_0 by that estimated from OLCI measurements (Kokhanovsky et al., 2019):

$$R_0 = R_{meas}^{z}(865nm)R_{meas}^{1-z}(1020nm), \tag{81}$$

where $z = (1-b)^{-1}$, $b = \sqrt{\frac{\alpha_{17}}{\alpha_{21}}}$, α_{17} is the bulk ice absorption coefficient at the channel 17 of OLCI (865nm), R_{meas} is the measured OLCI reflectance at a given OLCI channel.

The histogram of the coefficient of variance corresponding to the data shown in Fig.8 ais given in Fig.10. We see that the values of CV are smaller than 10% for most of cases. There are regions in Eastern Antarctica, where the deviations are below 5%. The areas with larger deviations could be due to the presence of clouds or structures on the snow surface not captured by the proposed model. The differences can be further decreased, if OLCI gains are used as discussed above.

Preprints (www.preprints.org) | NOT PEER-REVIEWED | Posted: 15 August 2022 doi:10.20944/preprints202208.0258.v1

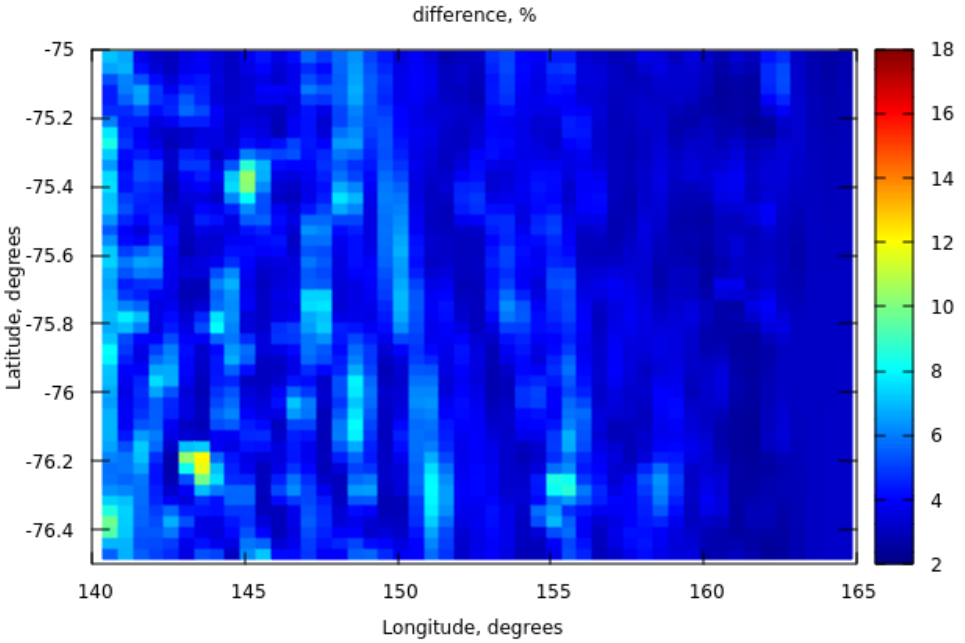

Fig.8. The difference (in percent, see Eq. (75)) between measured and modelled spectra.

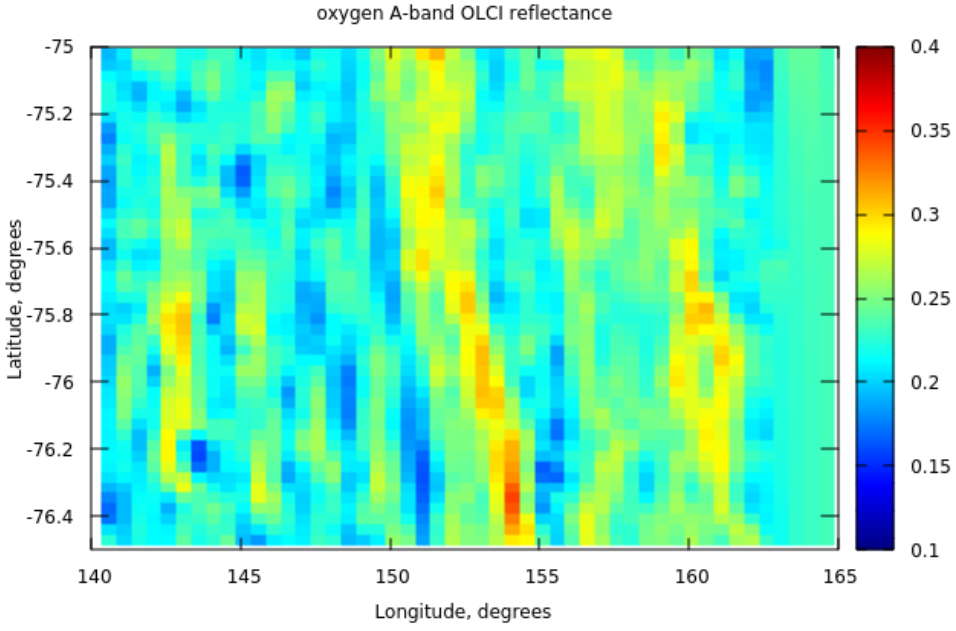

Fig.9. OLCI reflectance at 761.25nm for the case shown in Fig.8.

Preprints (www.preprints.org) | NOT PEER-REVIEWED | Posted: 15 August 2022 doi:10.20944/preprints202208.0258.v1

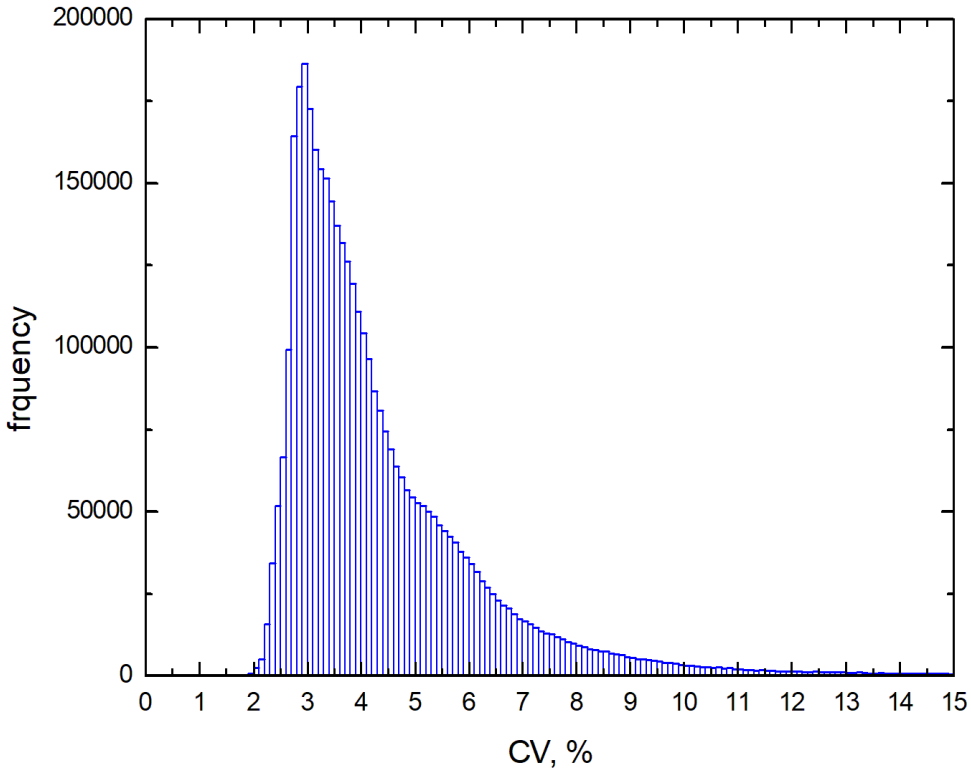

Fig.10. The statistical distribution of the error of the approximation.

4. Conclusions

In this work we have proposed an analytical relationship between clear sky top-of-atmosphere spectral reflectance as measured by a satellite instrumentation at moderate spectral resolution in the visible and near infrared regions of electromagnetic spectrum (400-1000nm) over extended snow surfaces such as existing in Antarctica. Both atmosphere and surface are relatively clean in Antarctica, which makes the solution of the studied problem possible. One can also apply the technique to other similar areas with underlying snow and ice surfaces (e.g., Greenland, Tibetan Plateau, etc.). Although the numerical solution of the radiative transfer equation leads to more accurate results as compared to those presented in this work, it does not mean that these results of a better accuracy as compared to experimental measurements of spectral reflectance. This is related to the fact that exact modelling of light reflectance from natural snow and ice surfaces as detected on a satellite is hardly possible because of various structures on the snow surfaces (e.g., sastrugi), close – packed media effects, layered nature and

Preprints (www.preprints.org) | NOT PEER-REVIEWED | Posted: 15 August 2022 doi:10.20944/preprints202208.0258.v1

complex microstructure of snow fields containing both external and internal impurities. The technique can be extended to larger wavelengths taking into account other absorption bands of atmospheric gases. Also Mie calculations (van de Hulst, 1981) or look up tables can be used for the spectral aerosol phase function and optical thickness in case atmospheric aerosol load is substantial and aerosol parameters are known in advance.

The spectral range 400-1000 nm is of special importance because the TOA reflectance is more sensitive to both snow and atmospheric aerosol properties as compared to longer wavelengths, where the contribution of atmospheric aerosol and molecular light scattering can be neglected and reflectance of light from snow decreases. The fast radiative transfer FORTRAN code for the calculation of the reflectance over snow (SNOWTRAN) can be freely downloaded from the site *https://sites.google.com/site/kokhanovsky2016/codes*.

5. Acknowledgements

This work has been supported by the European Space Agency (the EO Science for Society ESRIN CCN 4000125043/18/I-NB). The author is grateful to Sergey Korkin for providing the RT SORD code. The author thanks Jason Box, Carsten Brockmann, Luca Lelli and Thomas Wagner for the discussion of several topics related to this work.

6. References

Abramowitz, M., Stegun, I. (eds.), 1964: *Handbook of Mathematical Functions and Formulas, Graphs, and Mathematical Tables*, National Bureau of Standards Applied Mathematics Series, No. 55, U.S. Government Printing Office, Washington D. C.

Avaste, O.A., V. S. Atroshenko, 1960: The accuracy of the Sobolev approximation, *Izvestiya*, Geophysics, 3, 45-49.

Ångström, A., 1929: On the atmospheric transmission of Sun radiation and on dust in the air, *Geografiska Annaler*, 11, issue 2, 156–166.

Busbridge, I. W., S. E. Orchard, 1967: Reflection and transmission of light by a thick atmosphere according to a phase function $1+x\cos\upsilon$, *Astrophysics Journal*, 149, 655-664.

Cachorro, V. E., Antuña-Sanchez J. C., de Frutos A. M., 2022: SSolar-GOA v1.0: a simple, fast, and accurate Spectral solar radiative transfer for clear skies, *Geosci. Model Dev*., 15, 1689–1712, https://doi.org/10.5194/gmd-15-1689-2022.

Coakley, J., & Chylek, P. (1975). The two-stream approximation in radiative transfer: including the angle of the incident radiation. *Journal of the Atmospheric Sciences*, *32*, 409-418.

Gay, M., Fily, M., Genthon, C., Frezzotti, M., Oerter, H., and Winther, J.-G., 2002: Snow grain-size measurements in Antarctica, *J. Glaciol.*, 48, 527–535.

Gorshelev, V., Serdyuchenko, A., Weber, M., Chehade, W., and Burrows, J. P., 2014: High spectral resolution ozone absorption cross-sections – Part 1: Measurements, data analysis and comparison with previous measurements around 293 K, *Atmos. Meas. Tech*., 7, 609–624, https://doi.org/10.5194/amt-7-609-2014.

Green A. E. S., J. C, Wagner, and A. Mann, 1988: Analytic spectral functions for atmospheric transmittance calculations, *Applied Optic*s, 27, 11, 2266-2272.

Grenfell, T.C., S.G. Warren, and P.C. Mullen. Reflection of solar radiation by the Antarctic snow surface at ultraviolet, visible, and near-infrared wavelengths, 1994: *J. Geophys. Res.*, 99, 18669-18684.

Hansen, J. E. and Travis, L. D., 1974: Light scattering in planetary atmospheres, *Space Sci. Rev*., 16(4), 527–610, doi:10.1007/BF00168069.

Iqbal, M., 1983: *An Introduction to Solar Radiation*, Amsterdam: Elsiever.

Katkovsky, L.V.; Martinov, A.O.; Siliuk, V.A.; Ivanov, D.A.; Kokhanovsky, A.A., 2018: Fast atmospheric correction method for hyperspectral data, *Remote Sens.*, *10*, 1698. https://doi.org/10.3390/rs10111698

Katsev, I. L., Prikhach, A. S., Zege, E. P., Grudo, J. O., and Kokhanovsky, A. A., 2010: Speeding up the aerosol optical thickness retrieval using analytical solutions of radiative transfer theory, *Atmos. Meas. Tech*., 3, 1403–1422, https://doi.org/10.5194/amt-3-1403-2010.
Kokhanovsky A A and Eleonora P. Zege, 2004: Scattering optics of snow, *Appl. Opt*. 43, 1589-1602.

Kokhanovsky, A. A., Mayer, B. and Rozanov, V. V., 2005a: A parameterization of the diffuse transmittance and reflectance for aerosol remote sensing problems, *Atmos. Res*., 73(1–2), 37–43, doi:10.1016/j.atmosres.2004.07.004.

Kokhanovsky, A.A., 2005b: Reflection of light from particulate media with irregularly shaped particles, *Journal of Quantitative Spectroscopy and Radiative Transfer*, 96, Issue 1,1-10, https://doi.org/10.1016/j.jqsrt.2004.12.008.

Kokhanovsky, A.A., 2006: Cloud Optics, Berlin: Springer.

Kokhanovsky, A. A., et al., 2010: Benchmark results in vector atmospheric radiative transfer, *Journal of Quantitative Spectroscopy and Radiative Transfer*, 111, 1931-1946.

Kokhanovsky, A., Lamare, M., Di Mauro, B., Picard, G., Arnaud, L., Dumont, M., Tuzet, F., Brockmann, C. and Box, J. E., 2018: On the reflectance spectroscopy of snow, *Cryosphere*, 12(7), 2371–2382, doi:10.5194/tc-12-2371-2018.

Kokhanovsky, A., Lamare, M., Danne, O., Brockmann, C., Dumont, M., Picard, G., Arnaud, L., Favier, V., Jourdain, B., Meur, E. Le, Di Mauro, B., Aoki, T., Niwano, M., Rozanov, V., Korkin, S., Kipfstuhl, S., Freitag, J., Hoerhold, M., Zuhr, A., Vladimirova, D., Faber, A. K., Steen-Larsen, H. C., Wahl, S., Andersen, J. K., Vandecrux, B., van As, D., Mankoff, K. D., Kern, M., Zege, E. and Box, J. E., 2019: Retrieval of snow properties from the Sentinel-3 Ocean and Land Colour Instrument, *Remote Sens.*, 11(19), 1–49, doi:10.3390/rs11192280.

Kokhanovsky, A., Box, J. E., Vandecrux, B., Mankoff, K. D., Lamare, M., Smirnov, A. and Kern, M., 2020: The determination of snow albedo from satellite measurements using fast atmospheric correction technique, *Remote Sens.*, 12(2), 1–18, doi:10.3390/rs12020234.

Kokhanovsky, A., Iodice F., Lelli L., Zschaege A., De Quattro N., Gasbarra D., Retscher C., 2021a: Retrieval of total ozone column using high spatial resolution top-of-atmosphere measurements by OLCI/S-3 in the ozone Chappuis absorption band over bright underlying surfaces, Journal of Quantitative Spectroscopy and Radiative Transfer,276,107903,ISSN 0022-4073,https://doi.org/10.1016/j.jqsrt.2021.107903.

Kokhanovsky, A. A., et al., 2021b: Retrieval of dust properties from spectral snow reflectance measurements, *Frontiers in Environmental Science, Informatics and Remote Sensing* 9, https://www.frontiersin.org/article/10.3389/fenvs.2021.644551.

Kokhanovsky, A.A., 2021: *Snow optics*, Cham: Springer Nature.

Korkin, S., Lyapustin, A., Sinyuk A., Holben B., Kokhanovsky A., 2017: Vector radiative transfer code SORD: Performance analysis and quick start guide, *Journal of Quantitative Spectroscopy and Radiative Transfer*, 200, 295-310,https://doi.org/10.1016/j.jqsrt.2017.04.035.

Liou, K.-N., 2002: *An introduction to atmopsheric radiation*, N.Y.: Academic Press.

Malinka, A.V., Zege, E.P., Katsev, I.L., L. Istomina, 2016: Accounting for atmospheric effects in the interpretation of satellite and ground-based optical measurements. *J Appl Spectroscopy*, 83**,** 741–749, https://doi.org/10.1007/s10812-016-0357-3.

Mazeran, C., Rueskas, A., 2020: *Ocean Colour System Vicarious Calibration Tool Documentation*, EUMETSAT, EUM/19/SVCT/D2.

Mei, L., Rozanov, V. and J. P. Burrows, 2020: A fast and accurate radiative transfer model for aerosol remote sensing, Journal of Quantitative Spectroscopy and Radiative Transfer, 256,107270, https://doi.org/10.1016/j.jqsrt.2020.107270.

Mei, L., Rozanov V. , Jiao Z., Burrows J. P., 2022: A new snow bidirectional reflectance distribution function model in spectral regions from UV to SWIR: Model development and application to ground-based, aircraft and satellite observations, ISPRS Journal of Photogrammetry and Remote Sensing, 188, 269-285, https://doi.org/10.1016/j.isprsjprs.2022.04.010.

Picard, G., Libois, Q., and Arnaud, L., 2016: Refinement of the ice absorption spectrum in the visible using radiance profile measurements in Antarctic snow. *The Cryosphere* , 10, 2655–2672, https://doi.org/10.5194/tc-10-2655-2016.

Pierluissi, J. H., C.-M. Tsai, 1986: Molecular transmission band model for oxygen in the visible, *Applied Optics*, 25, 15, 2458-2460.

Preusker, R., Carbajal Henken, C., Fischer, J., 2021: Retrieval of daytime total column water vapour from OLCI measurements over land surfaces, *Remote Sens. 13*, 932, https://doi.org/10.3390/rs13050932

Ricaud, P., Gabard, B., Derrien, S., Chaboureau, J.-P., Rose, T., Mombauer, A. and Czekala, H., 2010 : HAMSTRAD-Tropo, A 183-GHz Radiometer Dedicated to Sound Tropospheric Water Vapour Over Concordia Station, Antarctica, *IEEE Transactions on Geoscience and Remote Sensing*, 48, 1365–1380, doi:10.1109/TGRS.2009.2029345.

 doi:10.20944/preprints202208.0258.v1

Six, D.; Fily, M.; Blarel, L.; Goloub, P. , 2005: First aerosol optical thickness measurements at Dome C (east Antarctica), summer season 2003–2004. *Atmos. Env.* , *39*, 5041–5050.

Sobolev, V. V., 1975: *Light scattering in planetary atmospheres*, Pergamon Press.

Tomasi, C., and Petkov, B. H. , 2015: Spectral calculations of Rayleigh – scattering optical depth at Arctic and Antarctic sites using a two – term algorithm, *J. Geophys. Res.* 10.1002/2015JD023575.

Tomasi, C., et al., 2010: Characterizing polar atmospheres and their effect on Rayleigh-scattering optical depth, *J. Geophys. Res.*, 115, D=2205, doi: 10.1029/2009JD012852.

van de Hulst, H.C., 1980: *Multiple Light Scattering*, v.1, New York: Academic Press.

van de Hulst, H.C. , 1981: *Light scattering by small particles*. New York: Dover.

Warren, S., and Brand, R. E., 2008: Optical constants of ice from the ultraviolet to the microwave: a revised compilation. *J. Geophysical Research* 2008, 113, D14, https://doi.org/10.1029/2007JD009744.

Wiscombe, W. J., and Grams, G. W., 1976: The backscattered fraction in two-stream approximations. *Journal of the Atmospheric Sciences*, *33*, 2440-2451.

Zege, E.P., A. P. Ivanov, and I. L. Katsev, 1991: *Image transfer through light scattering media*, Berlin: Springer.